Hydrothermal Alteration of Diatomite for Removal of Aqueous Cu^{2+}, Pb^{2+} and Zn^{2+}

Daniel Höllen[1], Dietmar Klammer[1], Ilse Letofsky-Papst[2] and Martin Dietzel[1]

1. *Institute of Applied Geosciences, Graz University of Technology, 8010 Graz, Austria*

2. *Institute for Electron Microscopy and Fine Structure Research, Graz University of Technolog., 8010 Graz, Austria*

Abstract: Natural unconsolidated diatomite was hydrothermally treated with a strongly alkaline aluminate solution at 100 and 125 °C to obtain high-value material for cation removal from aqueous solutions. Diatomite (D) alteration at 1 and 0.022 M of KOH and Al, respectively, leads finally to the formation of merlinoite (M). But coupled dissolution and precipitation yield in an intermediate amorphous potassium-rich alumosilica phase (IP), most conspicuous as 100 to 1,000 nm-sized spherules. All alteration products display high removal capacities for Cu^{2+}, Pb^{2+}, and Zn^{2+} from artificial and natural solutions. Interestingly the presence of the IP creates elevated surface areas and very high cation removal efficiencies up to 99.97 % without significant cation selectivity. In contrast a pronounced cation selectivity for the removal in the order of Pb^{2+} > Cu^{2+} > Zn^{2+} is stimulated by the occurrence of M, where removal capacities and surface areas are lower compared to alteration products with the dominance of the IP. Thus bio-opal in terms of frequently occurring diatomite can be efficiently transformed to a highly active composite material for Cu^{2+}, Pb^{2+}, and Zn^{2+} removal by hydrothermal treatment. Tailoring issues are referred to the formation of the IP versus zeolites and the apparent hierarchical micro- to nanostructures of diatomite and the reaction products, respectively.

Key words: Diatomite, zeolitisation, intermediate phase, merlinoite, heavy metal removal.

1. Introduction

Diatoms are up to ≈ 100 µm-sized algae and occur in nearly all aquatic ecosystems [1]. They consist of opaline cell walls with distinct micropore structures [2]. The accumulation and compaction of the siliceous parts of dead diatoms lead to the formation of a porous fine-grained sediment, so-called diatomite [1]. Diatomite is a widespread marine sediment, which preferentially occurs in depths of 4.5 to 6 km between the carbonate and opal compensation depths, respectively [3]. Individual porosities of diatomite vary

from 75vol.% to 85vol.% [4]. Although diatomite is mainly composed of opal, SiO$_2$·nH$_2$O, it may contain additional phases like carbonates and alumosilicates, which depend on the apparent sedimentary environment [5].

About 60% of the worldwide mined diatomite is used for rather traditional filtration issues [6]. The microporous structure provides excellent properties to retain suspended solids down to bacteria [1]. More recently various applications of diatomite have been established to create composite materials and tailored alteration products for different purposes [7]. For instance coatings of diatoms with metal oxides and hydroxides provide ceramic devices with extraordinarily high specific surface areas, e.g., for catalysts [8]. Diatoms are also extensively used as substrate for hydrothermal synthesis of silicates. In a rather simple approach diatomite is used as a silica source via dissolution, similar to the application of rice

Corresponding author: Daniel Höllen, Dipl.-Min., research associate, research fields: applied mineralogy and hydrogeochemistry. E-mail: daniel.hoellen@tugraz.at.

husk ash [9], fly ash [10], bottom ash [11] or pumice [12]. A wide range of diatom alteration products can be synthesized, e.g., mordenite [13], ZSM-5 [14], Na-P1, analcime, cancrinite, hydroxysodalite [15] and zeolite P [16]. In a more advanced approach diatoms are coated with zeolite nanoparticles as seeds for further tailored zeolite synthesis [17]. The formation of individual minerals and solids can be also triggered by organic templates [13], diatom pre-treatment [18] and physicochemical parameters like excess alkalinity [19] and temperature [15]. In the latter approaches the hierarchically structured composite material of the persisting micropores of diatoms and the newly formed nanopores of zeolites is highly challenging for applications for water treatment [20]. Partly zeolitised diatomite provides both the retention of suspended matter and the removing of cations such as heavy metals from the solution. Moreover the partly remaining primary microporosity of diatomite yields in proper flow behaviour of aqueous solutions through the composite material if packed columns are suggested for application in commercial products.

Previous studies on the hydrothermal alteration of diatomite are mostly focussed on the final products of zeolitisation and its technical application [21]. However the transformation of bio-opal to zeolite comprises complex reaction stages and kinetics, where amorphous or gel-like solids may be formed as intermediate phases. The occurrence of such kind of intermediate phases and their impact on water treatment issues are highly promising for economic aspects, like potential increase of cation removal efficiencies and cost-saving production, but still less explored. Therefore two sets of hydrothermal experiments were carried out to follow ongoing zeolitisation of diatomite. Subsequently the alteration products, which are obtained at individual reaction times, were tested for their removal of Pb^{2+}, Cu^{2+} and Zn^{2+} from solution as these heavy metals are highly relevant for geogenic and anthropogenic pollutions in aquatic environments.

2. Materials and Methods

2.1 Analytics

The chemical composition of aqueous solutions was analyzed by inductively coupled plasma optical emission spectroscopy (ICP-OES, Perkin Elmer Optima 4300) with an accuracy of ± 3% for K, Si, Al, Cu, Pb and Zn. pH was measured using a WTW Inolab 740 combined with the pH electrode BL 26 (Schott).

Solids were characterized by X-Ray diffraction analyses (XRD, PANalytical X'Pert Pro; Co Kα, 40 mA, 45 kV, sample rotation) between 4 and 110° (2θ) using the Rietveld refinement approach for quantification (PANanaytical X'Pert High Score Plus). Zincite (Johnson Matthey, spec. pure) was used as an internal standard for quantification of amorphous phases. Refinements usually lead to weighted R-values of about 7%. Imaging of solids was done by scanning electron microscopy (SEM, Zeiss DSM 982 Gemini). Therefore solid samples were coated with an Au-Pd alloy using a Scancoat Six sputter apparatus. Transmission electron microscopy (TEM, FEI Tecnai 12 for TEM-SAED, Philips CM20 for TEM-EDX) with energy-dispersive X-Ray spectroscopy (EDX) was used for space-resolved chemical analyses and selected area electron diffraction (SAED) for crystallographic analyses. X-Ray fluorescence spectroscopy (XRF, PANanalytical PW 2404) was applied to determine the chemical bulk composition of selected samples. BET analyses were conducted to estimate the specific surface area using a FlowCash II 2300 equipment with a nitrogen/helium mixture.

2.2 Materials

The diatomite used for hydrothermal alteration experiments originates from a northern African deposit and predominantly contains diatoms of the Centrales group (trade name Thiele, Fig. 1a, top left). The diatomite has a specific BET surface area of 12.6 m²·g⁻¹ and consists of 97 wt.% amorphous phase (opaline cell walls), 2 wt.% mica and 1 wt.% quartz. Its chemical
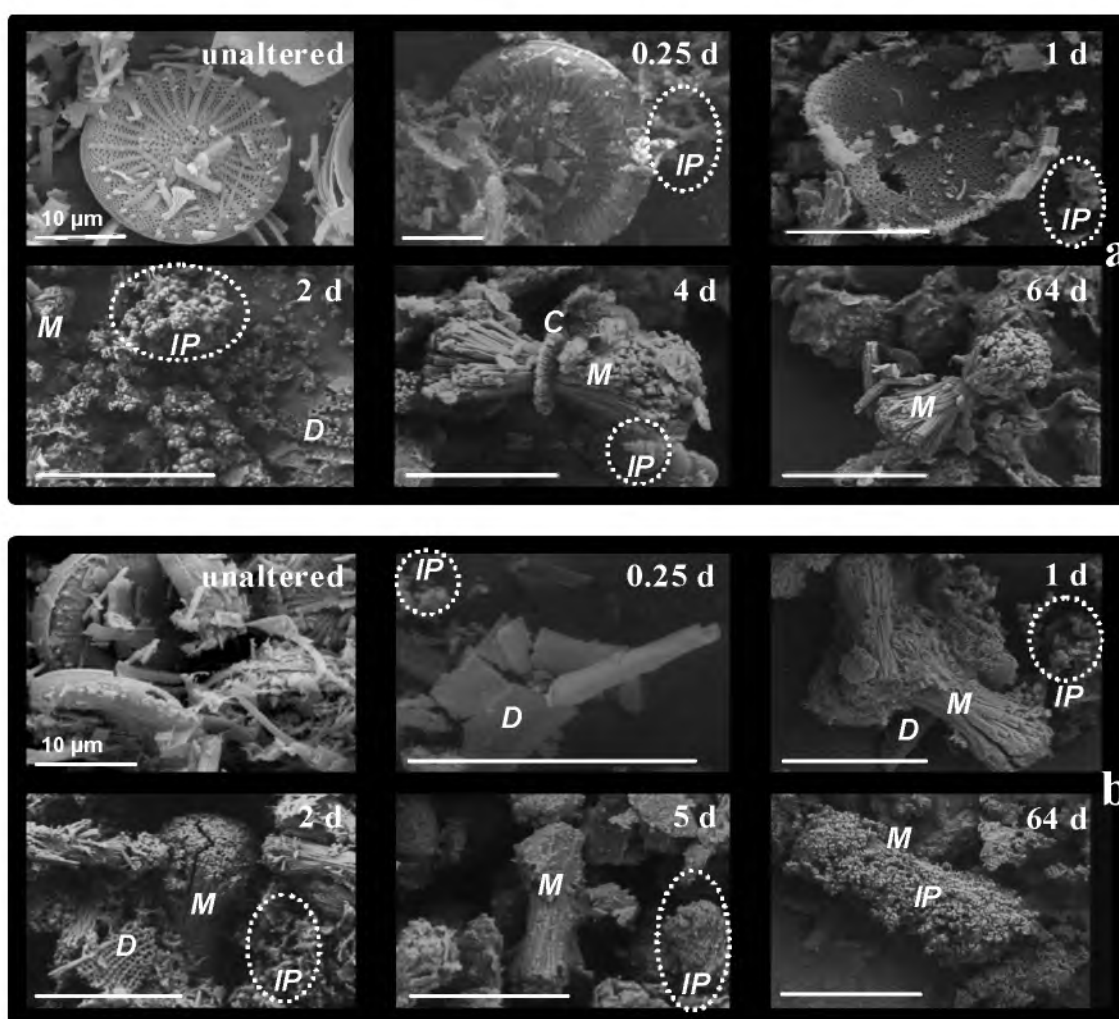
Fig. 1 SEM-SE images of unaltered diatomite and diatomite altered at 100 °C (a) and 125 °C (b) for distinct reaction times (0.25 d ≤ t_{syn} ≤ 64 d). D: diatom, IP: intermediate phase, M: merlinoite, C: chabazite.

composition is 93.3 wt.% SiO_2, 1.7 wt.% Al_2O_3, 0.8 wt-% Fe_2O_3, 0.2 wt.% MgO, 0.3 wt.% CaO, 0.3 wt.% K_2O and 3.5 wt.% L.O.I..

For the hydrothermal experiments an aluminium-containing stock solution was prepared by suspending 1 g of gibbsite (γ-Al(OH)$_3$, Merck p.a.) in 0.5 L of freshly prepared 1 M KOH in a gas-tight Nalgene® polycarbonate bottle to prevent CO_2 absorption. After a reaction time of seven days at a temperature of 50 °C the solution was cooled down to 25 °C and subsequently separated from the partly remaining gibbsite by membrane filtration (0.45 μm). The solution contains 0.022 M of Al mostly as $Al(OH)_4^-$ at pH 13.7 which represents still undersaturation with respect to gibbsite (saturation

index: $SI_{gibbsite}$ = -0.9 at 25°C; PHREEQC with database PhreeqC [22]). Since the solubility of gibbsite and amorphous aluminium hydroxide increases with temperature, no precipitation of $Al(OH)_3$ has to be expected by heating of the "pure" stock solution.

For cation removal experiments a stock solution was prepared which contains 0.5 mM of each Cu^{2+}, Pb^{2+}, and Zn^{2+}. Therefore $Pb(NO_3)_2$, $Zn(NO_3)_2 \cdot 4H_2O$ and $Cu(NO_3)_2 \cdot 3H_2O$ (Merck, p.a.) were dissolved in MilliQ water (pH 5). Moreover a drainage solution from a carbonate-hosted lead-zinc deposit in Carinthia (Austria) was used after membrane filtration (0.45 μm) for cation removal experiments. The latter solution contains 0.48 and 17 μM of Pb^{2+} and Zn^{2+}, respectively (pH 8).

2.3 Experimental Setup

Alteration experiments were conducted by placing 0.5 g of the untreated diatomite in 0.025 L of the alkaline aluminate stock solution in Teflon coated steel autoclaves (total volume 0.070 L) at 100 and 125 °C. For both temperatures eight autoclaves were loaded for tempering between 0.25 and 64 d. After distinct reaction times the autoclaves were cooled down to about 30 °C and the experimental solutions were immediately separated from the obtained solids by membrane filtration (0.45 μm) for analyses. The solids were rinsed with 0.2 L MilliQ water and dried at 40 °C before analyses. To achieve sufficient material for XRF analyses six additional but analogous experiments were carried out as discussed in chapter 3.1.2.

Heavy metal removal experiments were carried out with selected reaction products from the alteration experiments. The selection criterion was based on the time-resolved change in morphology and phase composition caused by hydrothermal treatment. In each removal experiment 0.05 g of the reaction product was suspended in 0.01 L of the heavy metal stock solution or drainage solution. Analogous experiments were conducted with unaltered diatomite to evaluate the impact of newly formed phases on the metal removal behavior. In all cases the suspensions were prepared in PP vials (0.01 L) and placed in a horizontal shaking device (E.B. KS-15) with a frequency of 250 min^{-1} for an experimental time of 3 d at 25 °C. In several pre-experiments the kinetics of metal removal from aqueous solutions by altered diatomite was checked: within the error of analyses constant concentrations of the remained Cu^{2+}, Pb^{2+} and Zn^{2+} in the experimental solutions were already reached at a reaction time of ≈ 0.5 d.

3. Results

3.1 Hydrothermal alteration of diatomite

3.1.1 Evolution of Reaction Products
SEM-SE images indicate the formation of an intermediate phase (IP) after hydrothermal treatment for 0.25 d, but most considerable at 2d and 1d at 100 and 125 °C, respectively (Fig. 1). The IP is most conspicuous as 100 to 1,000 nm-sized spherical particles and appears as aggregates spatially separated from the residual diatoms. IP spherules increase in size through reaction time, but still less sized IP particles can occur at elevated reaction times (e.g., 0.25d and 4 d in Fig. 1a; 100 °C). At a reaction time of 2 and 1 d for the 100 and 125 °C treatment, respectively, the formation of bundle-like aggregates with a length of about 10 μm is observed besides the IP. After 64 d of hydrothermal treatment the bundle-shaped solid is predominant in the sample for both temperatures (Fig. 1). In several cases the bundle-shaped solids are surrounded by a belt-like ring at their narrowest site (e.g. Fig. 1a; 4 d). Diatoms coexist with the IP and bundle-like aggregates, but completely disappear through hydrothermal treatment after 4 and 5 d (Figs. 1a and 1b, respectively).

XRD patterns (Fig. 2) evaluated by Rietveld refinement clearly reveal the formation of merlinoite (M) at a reaction time of 2 and 1 d at 100 and 125 °C, respectively, which coincides with the appearance of the above mentioned bundle-shaped solids. M was also identified by its tetragonal symmetry in SEM-SE images (Fig. 1). In two samples minor amounts of chabazite (C) are suggested from the XRD patterns (t_{syn} = 2 d and 4 d; Fig. 2a), but are rather hard to quantify due to coincidences with the XRD pattern of merlinoite.

Thus compositions of solids at distinct hydrothermal treatment intervals presented in Fig. 3 may include small proportions of C for the given content of M. The occurrence of both, M besides minor contents of C, as reaction product is in general accordance with the results from the hydrothermal treatment of fly ash with Al-rich alkaline solutions, where bundle-shaped M is documented to be partly associated with C forming the belt [23].

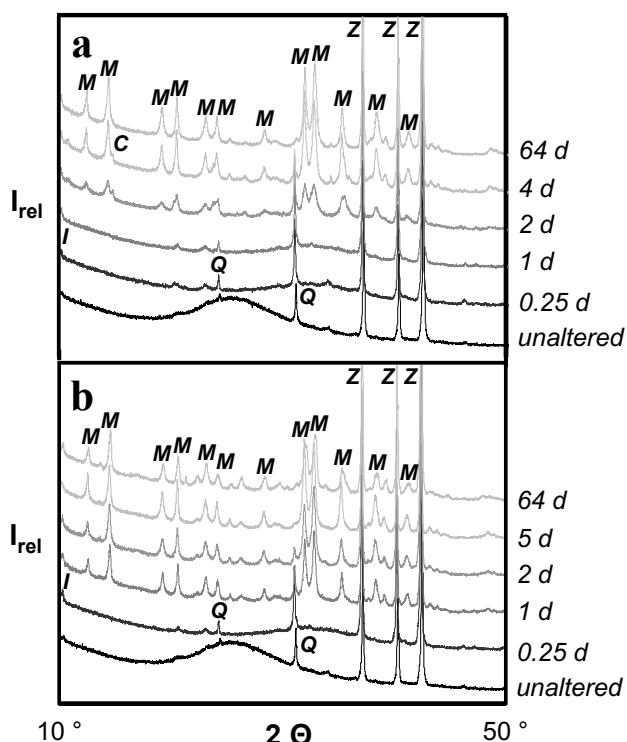Such a mineral association is obviously displayed in

Fig. 2 XRD patterns (Co-Kα) of unaltered diatomite and diatomite altered at 100 °C (a) and 125 °C (b) for distinct reaction times (0.25 d ≤ t_{syn} ≤ 64 d). M: merlinoite, C: chabazite, Q: quartz, I: illite/muscovite, Z: zincite (added as internal standard). Note: The increase of peak intensities for Q and I (both relicts) through alteration at t_{syn} = 0.25 d is caused by the preferential dissolution of diatoms.

Fig. 1a (tsyn = 4 h, 100 °C). However XRD patterns and SEM images suggest that this kind of zeolite association (C + M) is limited to reaction products at distinct alteration times (e.g., 2d to 4 d, 100 °C). The total zeolite content of the reaction product reaches values of 63 and 73 wt.% at 100 and 125°C, respectively (M in Fig. 3). At reaction times above 5 d the content of both, IP and M, remains more or less constant. It has to be pointed out that although IP is still present at the end of our experimental run, zeolites as M are likely to be the thermodynamically stable minerals at a final stage in such a highly alkaline environment [24].

3.1.2 Intermediate Phase

The IP is identified in the reaction products of hydrothermal treatment before M was formed after 2 d and 1 d at 100 and 125 °C, respectively (Fig. 3). As soon as M appears the concentration of the IP and D decreases, but the IP is still present even after a reaction time of t_{syn} = 64 h. The amorphous character of the IP suggested by XRD pattern of the bulk solid was verified by a TEM-SAED pattern given in Fig. 4.

A significant increase of the specific surface area from 12.6 to 37.8 and 31.0 m²·g⁻¹ at 100 and 125 °C, respectively, was obtained for unaltered to hydrothermally treated diatomite (t_{syn} = 0.25 d). The increase in specific surface area reflects the formation of the IP (Fig. 3). The latter values of the specific surface
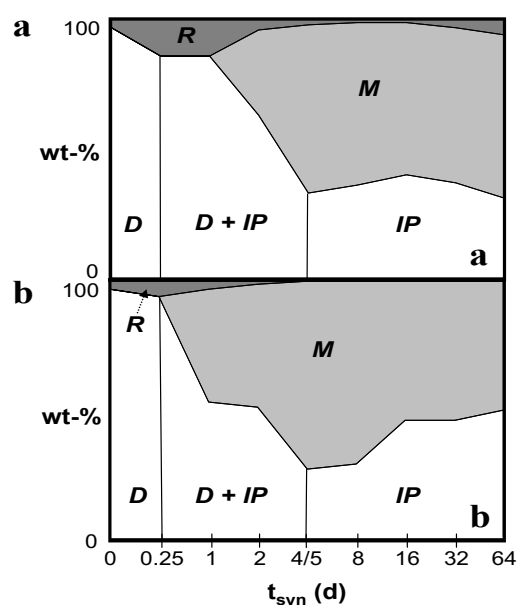

Fig. 3 Phase composition of unaltered diatomite and diatomite altered at 100 °C (a) and 125 °C (b) for distinct reaction times (0.25 d ≤ t_{syn} ≤ 64 d). D: diatom, IP: intermediate phase, M: merlinoite (partially including minor amounts of chabazite; Fig. 2a), R: relicts of quartz and illite/muscovite.
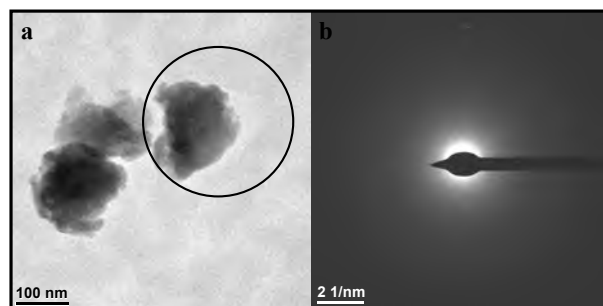

Fig. 4 TEM bright field image (a) and TEM-SAED pattern (b) of the intermediate phase in the reaction products of altered diatomite (t_{syn} = 2d at 100 °C).

for IP containing solids exceed also those of the zeolite-rich final reaction products which account for 18.3 and 15.0 m²·g^{-1} for 100 °C and 125 °C, respectively (t_{syn} = 16 d).

The chemical bulk composition of the IP-containing reaction products was calculated from the analyzed chemical composition of the coexisting solution as a function of reaction time (Al decreasing from 22 mM in the initial solution to 3 mM after alteration, Si increasing from zero to ~ 260 mM) and the initial amount of added solid (0.5 g of diatomite with 93 wt.% of SiO_2 and 1.7 wt.% of Al_2O_3) and liquid (0.025 L of 0.022 and 1 M of Al and KOH, respectively) (Fig. 5).

Individual Si and Al contents of the solids result from the uptake of dissolved and the release of fixed components. An exponential decrease in the calculated $(Si/Al)_s$ ratio of the bulk reaction product was obtained through reaction times up to 8 d where a rather constant value of about 1.2 is reached for t_{syn} > 8 d (Fig. 5). This trend in $(Si/Al)_s$ values is similar for both temperatures (100 and 125 °C) and obviously reflects the uptake of Al in the solid phase and the liberation of Si from the solid in the solution. In contrast the K content of the bulk reaction product could not be estimated through the ongoing alteration process as the decrease of K concentration at such a high concentration level was within the analytical precision. For experimental conditions, where the IP without zeolites is formed, six additional and analogous experiments were carried out to achieve sufficient IP containing material for XRF analyses (t_{syn} = 1 d at 100 °C). The directly measured $(Si/Al)_s$ ratio of 2 in this reaction product fits well with the calculated value between 3.1 and 1.2 in Fig. 6 and thus clearly supports the $(Si/Al)_s$ evolution during hydrothermal alteration of diatomite. As no zeolite is present at t_{syn} = 1 d a significant uptake of Al by IP is deduced.

The composition of individual IP particles was measured by single spot analyses by using TEM-EDX. The measured Si, Al, and K content of the IP is displayed in Fig. 5. The chemical composition of the IP

is mostly close to that of M and C ($(Si/Al)_s$ ≈ 2). Interestingly a second type of IP exists which displays a lower $(Si/Al)_s$ ratio close to 1 (Fig. 6).
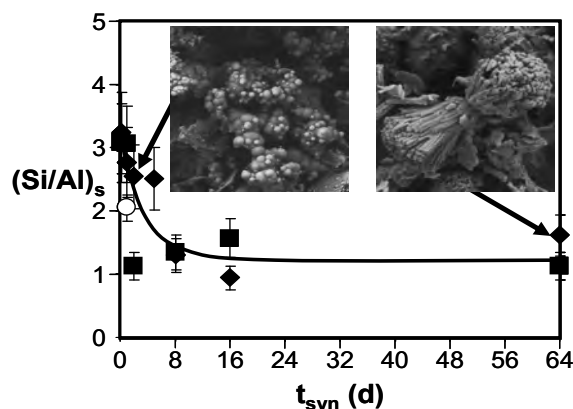

Fig. 5 Si/Al ratio of altered diatomite measured by XRF and calculated from the initial additions of solid and liquid, their chemical composition and the change of solution chemistry as a function of reaction time (0.25 d ≤ t_{syn} ≤ 64 d). ○: T = 100 °C, XRF; ♦: T = 100 °C, calculated; ■: T = 125 °C, calculated.
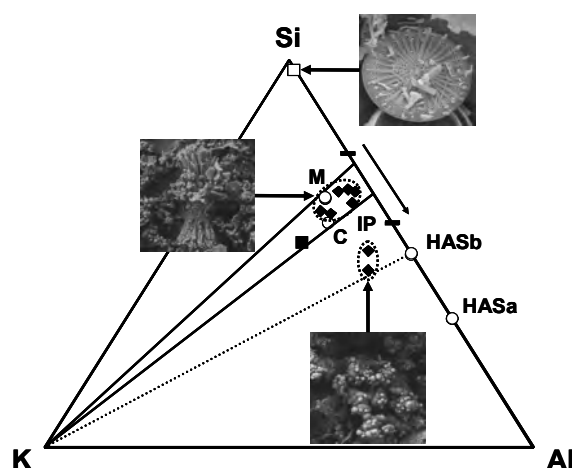

Fig. 6 Si-Al-K Triplot of the composition of unaltered diatomite and reaction products through diatomite alteration by hydrothermal treatment, solid lines indicate the range of the Si:Al ratio of merlinoite and chabazite, the dashed line indicates the minimal observed Si:Al ratio which equals that of HAS$_b$.
□: unaltered diatomite (D) by XRF bulk analyses; ■: altered diatomite (t_{syn}= 1 d) by XRF bulk analyses; ♦: intermediate phase (IP; t_{syn}= 2 d) by TEM-EDX spot analyses (250 nm in diameter); ○: merlinoite (M), chabazite (C), and hydroxyaluminosilicates (HASa and HASb) with ideal stoichiometry (see text); -: altered diatomite (approximated composition at the beginning and the end of the alteration process (connected with →), calculated from solution chemistry, Fig. 5).

3.2 Heavy Metal Removal Efficiency

Metal removal experiments clearly indicate that hydrothermal alteration products of diatomite yield very high efficiencies for removing Cu^{2+}, Pb^{2+} and Zn^{2+} from aqueous solutions. In the experiments with the 0.5 mM synthetic solution from 90 up to about 99.97 % of the initial dissolved metal ions are removed at 5 g·L^{-1} of suspended solid and in total 1.5 mM of Me^{2+} ions (Fig. 7). Thus ion exchange capacities of about 0.6 meq·g^{-1} are estimated for the reaction products. However the metal ion removal efficiencies reach maximum values for diatomite altered for t_{syn} = 0.25 and 1 d (at 125 and 100 °C, respectively). At these times of diatomite treatment the IP was detected and the specific surface area of the bulk material is highest (Section 3.2). Interestingly the cation removal efficiencies increase to about 99.97 % for the reaction products at t_{syn} = 0.25 d (Table 1) which contain no merlinoite but the IP (Figs. 1 and 3). As M becomes the dominant reaction product (t_{syn} = 4 and 5 d at 100 °C and 125 °C, respectively) the material is less efficient in the uptake of metal ions especially in the case of Cu^{2+} and Zn^{2+}. But the latter reaction products are more selective for cation removal in the order $Pb^{2+} > Cu^{2+} > Zn^{2+}$ compared to IP dominated products.

In respect to the mine drainage solution the reaction product at t_{syn} = 1 d at 100 °C was selected to test its cation removal behavior as this product displays highest cation removal efficiency for the synthetic Me-bearing solutions (Fig. 7). The respective experiments result in a decrease of Zn^{2+} and Pb^{2+} concentration from 17 to 0.12 μM and from 0.48 to < 0.04 μM, respectively. Thus even at the low heavy metal ion concentrations of the drainage solution compared to the synthetic Me-bearing solutions, high cation removal efficiencies for Zn^{2+} and Pb^{2+} are verified (99.9 and > 92 %, respectively). As the Zn^{2+} and Pb^{2+} concentrations, which remained after treatment with our reaction product, are significantly below the recommended or guideline values of drinking water of 45 and 0.05 μM, respectively [25], its
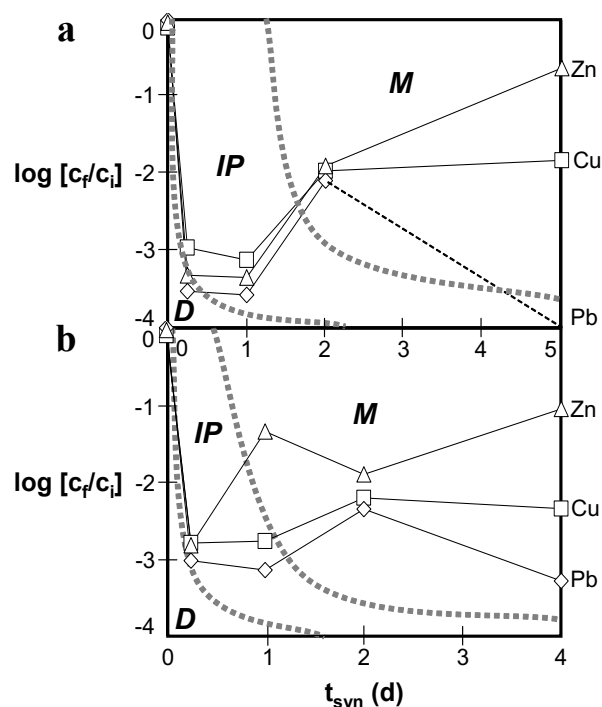

Fig. 7 **Cation removal capacities of unaltered diatomite (D) and diatomite altered for distinct reaction times (0.25 d ≤ t_{syn} ≤ 5 d) at 100 °C (a) and 125 °C (b) for Cu^{2+}, Pb^{2+}, and Zn^{2+}. c_i and c_f denote the initial and final molar metal concentrations in the solution. Dashed solid line: value of c_f is below the detection limit. Dotted lines: Schematical view of the predominance of diatomite (D), intermediate phase (IP), and merlinoite (M) within the alteration products.**

Table 1 **Cation removal capacities of unaltered diatomite and diatomite altered for distinct reaction times (0.25 d ≤ t_{syn} ≤ 5 d) for Cu^{2+}, Pb^{2+}, and Zn^{2+} at 100 and 125 °C. c_f: final molar metal concentration. t_{syn}: time for synthesis by hydrothermal treatment. bdl: below detection limit.**

t_{syn}	c_f			
d	μM			
100 °C	Cu	Pb	Zn	K
0	417	430	484	1517
0.25	0.566	0.150	0.245	4808
1	0.393	0.135	0.229	3811
2	5.70	4.13	6.44	4783
5	7.76	bdl	122	3325
125 °C				
0.25	0.835	0.473	0.765	4399
1	0.882	0.357	22.8	3913
2	3.26	2.24	6.44	5166
4	2.36	0.261	45.4	4425

extended application to the purification of drinking water is justified.

4. Discussion

4.1 Coupled Dissolution and Precipitation of Solids during Diatomite Alteration

The present alteration experiments of diatomite were carried out at strong alkaline conditions, where dissolution of opaline silica, as present in diatomite, is known to be fast and high concentrations of dissolved silica can be reached [26]. For instance [27] calculated a solubility of amorphous silica at pH 12 and 100 °C in the range of 100 mM of Si, which is lower than for our experimental results (~260 mM). However at the higher pH observed in our experiments (pH 13.6) the silica solubility can be simplified to be "unlimited" (Iler, 1979). The increase of silica solubility in alkaline solutions (pH > 9.5) is caused by the dissociation of monosilicic acid and the occurrence of negatively charged polysilicic acids (e.g., Ref. [28]). Thus the higher the pH, the stronger is the dissociation and the formation of polymers of silicic acid and thus the higher the solubility of silica. However in the presence of dissolved aluminum the dissolution of silica can be significantly retarded by the interaction of Al and Si [26]. Hydrothermal dissolution experiments of diatomite [29] indicate that even the replacement of Si by Al in diatomite significantly lowers its solubility.

In our study the Si concentration in the experimental solution is almost constant at 261 ± 23 mM at t_{syn} from 0.25 to 64d independent from temperature. This is curious as an increase in temperature from 100 to 125 °C should cause an increase Si solubility by a factor of about 10 in alkaline solutions [27]. We suggest that the constant Si concentration is caused by the formation of the metastable IP and zeolite minerals where the given Al content and not temperature is the limiting factor. In analogy Bouchiba, et al. [30] showed that in 1 M NaOH and at 80 °C the solubility of zeolite M is limited to about 20 mM of Si which is significantly lower than the solubility of amorphous silica at analogous conditions but without Al [26]. Thus in our experiments the less dissolution of amorphous silica compared to its "unlimited" solubility in the pure SiO_2-H_2O system at alkaline conditions is reasonable suggested to be caused by the reaction of Al with Si to build secondary colloids or solids (e.g., the IP or silicates) with slower dissolution kinetics or even lower solubility of silica.

Diatomite of similar size and shape compared to our material was used for hydrothermal zeolitisation by Du, et al. [16]. In contrast to our results they yield zeolite P as reaction product after hydrothermal treatment of diatomite in sodium-aluminate solution for 6 h at 90 °C. The significantly higher OH content in experiments of Du, et al. [16] (5 M NaOH) compared to our study (1 M KOH) involves higher silica solubility and stimulates zeolitisation which both may omit the formation of the metastable IP [31, 32].

Although zeolitisation of diatomite has already been conducted [13] and it is well known that amorphous precursors play a crucial role in zeolite formation [33], little attention has been paid to intermediate phases. As far as we know this is the first time where the formation of an amorphous Si-, Al- and K-containing intermediate phase through hydrothermal treatment of diatomite is documented which finally results in zeolitisation. Well documented primary reaction products of Si and Al in solution are the so-called amorphous hydroxyaluminosilicates (HAS) [34]. HAS can be formed e.g. by the adsorption of dissolved Al on amorphous silica [35, 36]. Similar reaction mechanisms might be valid in our experiments for the formation of the IP. In Fig. 6 the chemical compositions of two distinct HAS phases, HAS_a, and HAS_b, which are known to be formed as Al-Si intermediate or precursor phases, are displayed within the Si-Al-K triplot. The HAS_b phase is characterized by a $(Si/Al)_s$ ratio of 1 [37], which fits quite well with the Al-rich type of IP displayed in Fig. 6. In analogy to our results HAS phases can bound potassium ions [38]. X-ray amorphous K-aluminosilicates are also documented in hydrothermal synthesis of zeolites from K-aluminate and K-silicate solutions [39].

The results clearly indicate that through the formation of the metastable IP the available Al and Si is partly bounded in the reaction product before zeolite formation is induced. The range of IP compositions in our study may provide evidence for the chemical evolution of the IP during hydrothermal treatment. Since bulk composition of the reaction product changes from $(Si/Al)_s$ of about 2-3 (close to the value of C and M) to about 1 (value of HAS_b) we suggest that in particular HAS type IP particles survive, whereas other dissolve or are transformed to zeolite, e.g., by structural rearrangement [40]. Thus amorphous silica with low Al content may be more suitable for M formation than the HAS type IP (rich in Al), as supported by the direct replacement of amorphous silica by zeolites at extremely alkaline pH in anthropogenic soils [41] and on the other side by the high metastability of HAS [34].

4.1 Metal Ion Removal Behavior and Its Application

Metal ion exchange between an aqueous solution and a solid by adsorption or intercalation can be described as a competitive reaction where metal ion removal from the solution is associated with a simultaneous release of cations such a K and vice versa. This principle behavior can be followed by the K ion content of the solution for all metal removal experiments independent from the reaction product (Table 1). As weakly altered diatomite with elevated specific surface area leads to highest metal ion removal efficiencies, it is obvious that IP-dominated reaction products are most efficient for removing metal ions from aqueous solution (Fig. 7, Table 1). The respective decrease of the individual metal ions in the solution is similar for Cu^{2+}, Pb^{2+} and Zn^{2+}. In contrast the predominance of M versus IP in intensely altered diatomite (t_{syn} = 4 or 5 d) indicates an increase in cation uptake selectivity in the order of $Pb^{2+} > Cu^{2+} > Zn^{2+}$ (Fig. 7).

The selectivity of M for Pb^{2+} compared to Cu^{2+} and even more for Zn^{2+} can be explained by the fitting of these ions into the crystal structure of M which is characterized by cages surrounded by eight SiO_4 tetrahedra. The diameter of such a cage can be calculated assuming a regular octagon and subtracting the covalent oxygen radius and accounts for 148 pm. Hence M-rich alteration products favor Pb^{2+} (132 pm) which is quite similar as the initially incorporated K^+ (133 pm) compared to Zn^{2+} (82 pm) and Cu^{2+} (73 pm) due to their different ionic radii [19]. Moreover exchange rates in respect to (de)hydration of aqueous ions increase in the order of $Pb^{2+} > Cu^{2+} > Zn^{2+}$ [42] which may stimulate ion exchange kinetics for Zn^{2+} versus Cu^{2+} and Pb^{2+}.

5. Conclusions

Hydrothermal alteration of bio-opal such as diatomite in alkaline solutions can lead to the formation of zeolites which is well documented by a huge number of experimental approaches [15-17]. In the present study the time-resolved analyses of the hydrothermal alteration process of diatomite clearly reveal amorphous intermediate phases (IP) containing Al, Si and K. As far as we know this is the first time where the formation of an amorphous Si-, Al- and K-containing intermediate phase (IP) through hydrothermal alteration of diatomite is detected which finally results in zeolitisation.

The IP-rich reaction product is more efficient for the removal of metal ions from aqueous solutions compared to the merlinoite(M)-rich product. A non-selective ion exchange mechanism is suggested to be valid for the uptake of Cu^{2+}, Pb^{2+} and Zn^{2+} for IP which is governed by the provided solid surface area. In contrast the M-dominated reaction product is typically characterized by an ion-selective exchange mechanism. The advantages of such kind of diatomite-IP composites are (1) persisting micropores of diatoms for the retention of suspended matter down to bacteria and for proper flow behaviour of aqueous solutions and (2) very high removing efficiencies for metal ions from the solution. Challenging issues for ongoing and future studies comprise tailoring issues for

the formation of the IP within a hierarchically structured diatomite-IP composite material by adjusting T, pH and reaction time. As the IP is shown to be more efficient in cation removal from aqueous solution than the zeolite (M), shorter alteration times of diatomite to form the IP versus zeolite result in higher efficiencies of the reaction product and advanced economics for production.

Acknowledgments

References

[1] J.P.S. Smol, F. Eugene, The diatoms: Applications for the environmental and earth sciences, Cambridge University Press, 2010.

[2] E.V. Armbrust, The life of diatoms in the world's oceans, Nature 459 (2009) 185-192.

[3] M.E. Tucker, Sedimentary Petrology, An Introduction, Blackwell Scientific Publications, 1981.

[4] G.B. Cleveland, Diatomite carlifornia division of mines and geology bulletin 191 (1966) 151-158.

[5] E.R. Cressman, Non-detrital siliceous sediments, US Geological Survey Professional Paper, 440-T (1962) T1-T23.

[6] S. Moores, Blood, sweat and beers, filtration minerals reviewed, Industrial Minerals 484 (2008) 34-40.

[7] I.C. Gebeshuber, H. Stachelberger, M. Drack, Diatom bionanotribology biological surfaces in relative motion: their design, friction, adhesion, lubrication and wear, Journal of Nanoscience and Nanotechnology 5 (2005) 79-87.

[8] P.J.H. Harbour, P.G. Hartly, Metal Oxide/hydroxide materials, US, Patent, 2007/0281854A1, 2007.

[9] H.P. Wang, K.S. Lin, Y.J. Huang, M.C. Li, L.K. Tsaur, Synthesis of zeolite ZSM-48 from rice husk ash, Journal of Hazardous Materials 58 (1998) 147-152.

[10] H. Höller, U. Würsching, Zeolite formation from fly ash, Fortschritte der Mineralogie 63 (1985) 21-43.

[11] R.P. Penilla, A.G. Bustos, S.G. Elizalde, Zeolite synthesized by alkaline hydrothermal treatment of bottom ash from combustion of municipal solid wastes, Journal of the American Ceramic Society 86 (2003) 1527-1533.

[12] C.D. Johnson, F. Worrall, Zeolitisation of pumice-microporous materials on macroporous support structures derived from natural materials, Journal of Materials Chemistry 17 (2007) 476-484.

[13] V. Sanhueza, U. Kelm, R. Cid, Synthesis of mordenite from diatomite: A case of zeolite synthesis from natural material, Journal of Chemical Technology and Biotechnology 78 (2003) 485-488.

[14] V. Sanhueza, U. Kelm, R. Cid, L.E. Leopoldo, Synthesis of ZSM-5 from diatomite: A case of zeolite synthesis from a natural material, Journal of Chemical Technology and Biotechnology 79 (2004) 686-690.

[15] A. Chaisena, K. Rangsriwatananon, Synthesis of sodium zeolites from natural and modified diatomite, Materials Letters 59 (2005) 1474-1479.

[16] Y. Du, S. Shi, H. Dai, Water-bathing synthesis of high-surface-area zeolite P from diatomite, Particuology 9 (2011) 174-178.

[17] M.W. Anderson, S.M. Holmes, R. Mann, P. Foran, C.S. Cundy, Zeolitisation of diatoms, Journal of Nanoscience and Nanotechnology 5 (2005) 92-95.

[18] K. Pimraksa, P. Chindaprasirt, A. Rungchet, K. Sagoe-Crentsil, T. Sato, Lightweight geopolymer made of highly porous siliceous materials with various Na_2O/Al_2O_3 and SiO_2/Al_2O_3 ratios, Materials Science and Engineering A 528 (2011) 6616-6623.

[19] A. Bieniok, K. Bornholdt, U. Brendel, W.H. Baur, Synthesis and crystal structure of zeolite W, resembling the mineral merlinoite, J. Mater. Chem. 6 (1996) 271-275.

[20] D. Losic, J.G. Mitchell, N.H. Voelcker, Diatomaceous lessons in nanotechnology and advanced materials, Advanced Materials 21 (2009) 2947-2958.

[21] O.H. Ramírez, P.I. Hill, D.J. Doocey, S.M. Holmes, Removal and immobilisation of cobalt ions by a novel, hierarchically structured, diatomite/zeolite y composite, Journal of Materials Chemistry 17 (2007) 1804-1808.

[22] D.L. Parkhurst, C.A.J. Apello, User's guide to PHREEQC (V2), U.S. Geol. Sur, 1999, p. 312.

[23] B. Konrad, Experimental formation of zeolites by transformation of perlite, Faculty of Natural Sciences, Ph.D., Thesis, Karl-Franzens-Universität Graz, Graz, 1989. (In German)

[24] R.J. Donahoe, J.G. Liou, B.S. Hemingway, Thermochemical data for merlinoite: part 2. Free energies of formation at 298.15 K of six synthetic samples having various Si/Al and Na/(Na+K) ratios and application to saline, alkaline lakes, American Mineralogist 75 (1990) 201-208.

[25] WHO, Guidelines for drinking-water quality, in: World Health Organization (Ed.) World Health Organization, 2011.

[26] R.K. Iler, The Chemistry of Silica, John Wiley & Sons, 1979, p. 40-49.

[27] B.A. Fleming, D.A. Crerar, Silicic acid ionization and

calculation of silica solubility at elevated temperature and pH application to geothermal fluid processing and reinjection, Geothermics 11 (1982) 15-29.

[28] M. Dietzel, I.L. Papst, Stability of magadiite between 20 and 100 °C, Clays and Clay Minerals 50 (2002) 657-666.

[29] S. Dixit, P. Van Cappellen, A.J. Van Bennekom, Processes controlling solubility of biogenic silica and pore water build-up of silicic acid in marine sediments, Marine Chemistry 73 (2001) 333-352.

[30] N. Bouchiba, M.L.A.G. Castillo, A. Bengueddach, F. Fajula, F.D. Renzo, Zeolite metastability as a function of the composition of the surrounding solution: The case of faujasite and zeolite omega, Microporous and Mesoporous Materials 144 (2011) 195-199.

[31] C. Amrhein, G.H. Haghnia, T.S. Kim, P.A. Mosher, R.C. Gagajena, T. Amanios, et al., Synthesis and properties of zeolites from coal fly ash, Environmental Science and Technology 30 (1996) 735-742.

[32] A. Baccouche, E. Srasra, M.E. Maaoui, Preparation of Na-P1 and sodalite octahydrate zeolites from interstratified illite-smectite, Applied Clay Science 13 (1998) 255-273.

[33] T. Wakihara, S. Kohara, G. Sankar, S. Saito, M.S. Sanchez, A.R. Overweg, et al., A new approach to the determination of atomic-architecture of amorphous zeolite precursors by high-energy X-ray diffraction technique, Physical Chemistry Chemical Physics 8 (2006) 224-227.

[34] F.J. Doucet, C. Schneider, S.J. Bones, A. Kretchmer, I. Moss, P. Tekely, et al., The formation of hydroxyaluminosilicates of geochemical and biological significance, Geochimica et Cosmochimica Acta 65 (2001) 2461-2467.

[35] H.E. Mason, R.S. Maxwell, S.A. Carroll, The formation of metastable aluminosilicates in the Al_2O_3-SiO_2-H_2O system: Results from solution chemistry and solid-state NMR spectroscopy, Geochimica et Cosmochimica Acta 75 (2011) 6080-6093.

[36] I. Nishida, Y. Shimada, T. Saito, Y. Okaue, T. Yokoyama, Effect of aluminum on the deposition of silica scales in cooling water systems, Journal of Colloid and Interface Science 335 (2009) 18-23.

[37] C. Schneider, F. Doucet, S. Strekopytov, C. Exley, The solubility of an hydroxyaluminosilicate, Polyhedron 23 (2004) 3185-3191.

[38] K.W. Perrott, Effects of pH and aluminosilicate composition on KMg exchange selectivity of amorphous aluminosilicates, Geoderma 26 (1981) 311-322.

[39] C. Kosanović, I. Buljan, S. Bosnar, B. Subotić, N.N. Tušar, A. Ristić, et al., Thermal transformation of various potassium aluminosilicate precursors, Acta Chimica Slovenica 55 (2008) 960-965.

[40] C.E. White, J.L. Provis, T. Proffen, J.S.J. Van Deventer, Quantitative mechanistic modeling of silica solubility and precipitation during the initial period of zeolite synthesis, Journal of Physical Chemistry C 115 (2011) 9879-9888.

[41] D. Sauer, W. Burghardt, The occurrence and distribution of various forms of silica and zeolites in soils developed from wastes of iron production, Catena 65 (2006) 247-257.

[42] W. Stumm, Chemistry of the Solid-Water Interface, John Wiley & Sons, 1992, p. 428.